Forward Looking GPR-Based Landmine Detection Using a Robust Likelihood Ratio Test

Afief D. Pambudi*‡, Michael Fauß*, Fauzia Ahmad†, Abdelhak M. Zoubir*‡

*Signal Processing Group
Technische Universität Darmstadt
Merckstr. 25, 64283 Darmstadt, Germany
{apambudi, fauss}@spg.tu-darmstadt.de

†ECE Department
Temple University
Philadelphia, PA 19122, USA
fauzia.ahmad@temple.edu

‡Graduate School CE
Technische Universität Darmstadt
Dolivostr. 15, 64293 Darmstadt, Germany
{pambudi, zoubir}@gsc.tu-darmstadt.de

***Abstract*—We propose a robust likelihood ratio test to detect landmines using forward-looking ground penetrating radar. Instead of modeling the distributions of the target and clutter returns with parametric families, we use a kernel density estimator to construct a band of feasible probability densities under each hypothesis. The likelihood ratio test is then devised based on the least favorable densities within the bands. This detector is designed to maximize the worst-case performance over all the feasible density pairs and, hence, does not require strong assumptions about the clutter and noise distributions.**

***Index Terms*—Forward looking ground penetrating radar, landmine detection, robust probability ratio test, band model.**

I. Introduction

A forward-looking ground penetrating radar (FL-GPR) offers the potential of detecting landmines and unexploded ordnance with reduced risk to the operator [1]–[4]. This is accomplished with a large standoff distance between the detector and the targets, rendering it an attractive option compared to a conventional downward-looking radar that incurs the chance of disturbing and damaging the target scene. However, a challenge of using FL-GPR is that the illuminating signals and the reflected signals experience substantial attenuation owing to the near cancellation of the direct and ground-reflected waves. Furthermore, the interface roughness and subsurface clutter, which are usually highly non-stationary, have a strong impact on FL-GPR. Hence, in order to reduce the probability of detection errors, these effects need to be compensated with a proper signal processing method.

In this paper, we propose a pixel-wise likelihood ratio test (LRT) to detect landmines in the image domain. In contrast to existing approaches, we design the test to be robust against statistical model deviations [5]. More precisely, instead of modeling the distributions of the pixel intensity under each hypothesis with a parametric family of distributions, we use training data to construct two feasible bands within which the probability density functions (pdf) under either hypothesis are assumed to lie. The detector is then designed such that it minimizes the maximum error probability for all possible density pairs within the two bands. The existence of a minimax optimal test for this uncertainty model has been shown in [6]–[8]. The reason for following this approach is that accurate estimation of the clutter distribution, given its non-stationary behavior, is highly challenging. The proposed robust approach overcomes this problem since it does not require high estimation accuracy and is guaranteed to perform well over an entire non-parametric set of possible distributions.

The authors would like to thank Dr. Traian Dogaru of US Army Research Lab for providing the simulated data.

The work of A. D. Pambudi is supported by the 'Excellence Initiative' of the German Federal and State Governments and the Graduate School of Computational Engineering at Technische Universität Darmstadt and also supported by Deutsche Akademische Austauschdienst (DAAD)-Indonesian German Scholarship Programme.

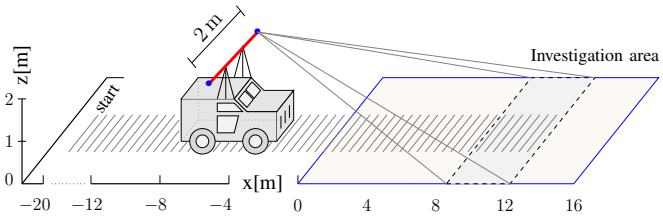

Fig. 1: Schematic of the FL-GPR vehicle-based system.

II. FL-GPR System & Measurement Configuration

We work with numerical data simulated using the Near-Field Finite-Difference Time-Domain software package, NAFDTD, developed by the U.S. Army Research Laboratory (ARL) [2]. Fig. 1 illustrates the FL-GPR system equipped with a $2\,\mathrm{m}$ antenna array mounted on top of a vehicle at the approximate height of $2\,\mathrm{m}$. The antenna array is composed of two transmit elements (blue dots) placed at the ends and 16 uniformly spaced receive elements (red line). The FL-GPR system operates in forward-looking mode from $x = -20\,\mathrm{m}$ to $x = 11\,\mathrm{m}$, sensing the investigation area at grazing angle $\theta_g \in [5°, 20°]$ approximately with a stepped frequency signal covering the 0.3 – $1.5\,\mathrm{GHz}$ band in $6\,\mathrm{MHz}$ increments.

Fig. 2 depicts the measurement configuration considered in the simulation. The investigation area contains nine landmines. Six landmines are buried at a depth of $3\,\mathrm{cm}$, five of them are metallic land-mines (1, 3, 4, 6, 7) and one is made of plastic (9). The remaining targets, two plastic land mines (2 and 8) and a metallic one (5), are placed on the surface. The

978-9-0827-9703-9/19/$31.00 ©2019 IEEE

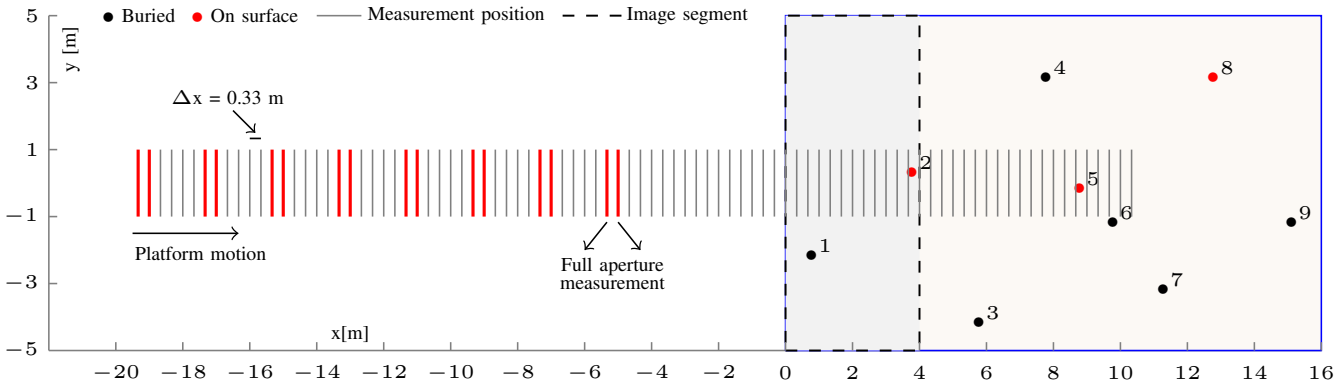

Fig. 2: The FL-GPR measurement configuration. The investigation area (blue rectangle) contains nine targets. The first image segment (dashed rectangle) is constructed by integrating eight full aperture measurements (red lines). Landmines: {1} metallic anti-personnel, {2,8} plastic anti-personnel, {3,6,7} metallic 155 mm shell, {4,5} metallic anti-tank, {9} plastic anti-tank.

plastic landmines are characterized with the relative dielectric constant $\varepsilon_r = 3.1$ and conductivity $\sigma = 2\,\mathrm{mS/m}$. The ground is modeled as a dielectric medium which is non-dispersive, non-magnetic, and homogeneous with ε_r = 6 and $\sigma = 10\,\mathrm{mS/m}$. The surface roughness is described as a 2-D Gaussian random process parameterized by the root mean square height $h_{\mathrm{rms}} = 0.8\,\mathrm{cm}$ and the correlation length $l_c = 14.26\,\mathrm{cm}$ [3].

We consider a total of 90 measurement positions depicted as parallel lines in Fig. 2. A full aperture measurement is realized over two adjacent measurement positions. In each position, we activate only one transmit element while all receive elements record the reflected signal from the scene. We obtain an image segment by integrating eight full aperture measurements. As an example, the 16 lines show the positions of eight full aperture measurements from $-19.33\,\mathrm{m}$ to $-5\,\mathrm{m}$ which are used to construct the first image segment (dashed rectangle). The second, third, and fourth image segments are obtained by integrating full aperture measurements from -15.33 to $-1\,\mathrm{m}$, -11.33 to $3\,\mathrm{m}$, and -7.33 to $7\,\mathrm{m}$ respectively, which however, are not depicted in Fig. 2. A tomographic image is thus constructed by integrating 32 full aperture measurements from $\mathrm{x} = -19.33\,\mathrm{m}$ to $\mathrm{x} = 7\,\mathrm{m}$ and is shown in Fig. 3.

The image in Fig. 3 is normalized to $40\,\mathrm{dB}$ dynamic range and consists of $N_{\mathrm{x}} = 1153$ pixels in downrange and $N_{\mathrm{y}} = 721$ pixels in crossrange with a resolution of $5\,\mathrm{cm}$. The landmines located near the boundary of the investigation area are less apparent since they are outside of the antenna's main lobe; the physical aperture width is shorter than the image crossrange (y-dimension). Compared to the landmines placed on the surface, the buried landmines are generally more challenging to discern due to the clutter caused by the radar back-scatter from the rough ground surface. In general, recognizing a plastic landmine is harder than a metallic one, since its return signal energy is comparable to that of the clutter. In order to improve the detection performance, we generate ten additional images by successively moving the radar closer to the target area. Compared to the image in

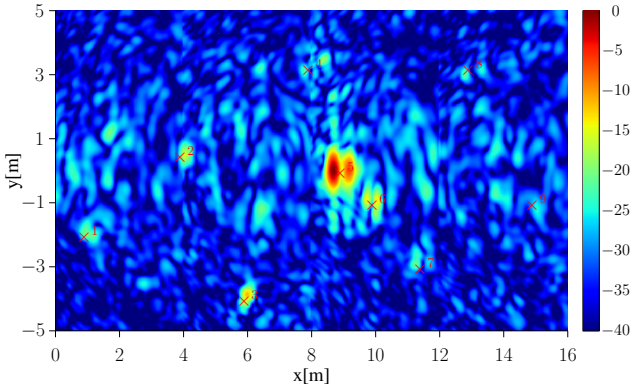

Fig. 3: Tomographic image from the first viewpoint.

Fig. 3 corresponding to the farthest viewpoint, the tomographic image from the viewpoint closest to the scene is realized by integrating measurements from $\mathrm{x} = -16\,\mathrm{m}$ to $\mathrm{x} = 10.33\,\mathrm{m}$. Therefore, we have $M = 11$ tomographic images available from various viewpoints to perform the LRT.

III. Image Domain Likelihood Ratio Test

A tomographic image is represented as a two dimensional array of normalized pixel intensities

$$x(i,j), \quad 1 \le i \le N_{\mathrm{x}}, \;\; 1 \le j \le N_{\mathrm{y}},$$

where $x(i,j) \in [0,1]$. The detection problem is to decide whether a pixel at (i,j) belongs to a target or is clutter. The problem can be defined as a test between a null and an alternative hypotheses as follows

$$H_0 : \; x(i,j) = \text{clutter pixel},$$
$$H_1 : \; x(i,j) = \text{target pixel}.$$

The proposed robust test, as well as the existing parametric LRT [3], [4], which is used as a reference for comparison, are based on the Neyman–Pearson approach [9] to optimal test design. That is, the test is designed such that it minimizes the

miss detection (type II error) probability under a constraint on the false alarm (type I error) probability. In other words, it minimizes the probability of confusing a target pixel for a clutter pixel for a given probability of confusing a clutter pixel for a target pixel. In order to highlight the similarities and differences between the parametric and the robust LRT, we briefly summarize the former before detailing the latter.

A. Parametric Test

Under the assumption that the tomographic images from different viewpoints are independent and identically distributed, a pixel wise LRT is given by

$$L(i,j) = \prod_{m=1}^{M} \frac{p_1(x_m(i,j))}{p_0(x_m(i,j))} \underset{H_0}{\overset{H_1}{\gtrless}} \gamma, \tag{1}$$

where $p_k(x_m(i,j))$ are the conditional probability density functions of the m-th tomographic image under hypotheses H_k, $k = 0, 1$. The threshold γ is determined based on the false alarm constraint α

$$\alpha = \int_{\gamma}^{\infty} f_L(l|H_0)\, dl, \tag{2}$$

where $f_L(l|\, H_0)$ is the density of the likelihood ratio L under the null hypothesis. In [3], [4], the authors show that the pixel intensities approximately follow a Rayleigh distribution under H_0 and a Gaussian mixture distribution under H_1. The corresponding density functions are given by

$$\begin{aligned} p_0(x) &= x\,/\sigma_0^2 \cdot \exp\left(-x\,/2\sigma_0^2\right), \\ p_1(x) &= \sum_{n=1}^{K} \omega_n\, \mathcal{N}(x \mid \mu_n, \sigma_n^2), \end{aligned} \tag{3}$$

where $\mathcal{N}(\bullet \,|\, \mu, \sigma^2)$ denotes a Gaussian distribution with mean μ and variance σ^2, K is the number of Gaussian distributions in the mixture, and $\omega_1, \ldots, \omega_K$ are mixture weights. Based on this model, the authors in [3], [4], [10] propose a generalized LRT, i.e., the test statistic in (1) is evaluated by replacing all unknown parameters in (3) with their maximum likelihood estimates.

B. Robust Test

The idea of minimax robust hypothesis testing is to design a test such that it works well under all feasible distributions. That is, in contrast to the generalized LRT, which tries to *reduce* the uncertainty by estimating unknown parameters, a minimax robust test *tolerates* uncertainty.

We start by considering the general case of two composite hypotheses

$$\begin{aligned} H_0 &: \; P \in \mathcal{F}_0, \\ H_1 &: \; P \in \mathcal{F}_1, \end{aligned} \tag{4}$$

where $\mathcal{F}_0$ and $\mathcal{F}_1$ are two disjoint sets of feasible distributions which are chosen such that they adequately capture the distributional uncertainties of the underlying detection problem. Here, we use Kassam's band model for this purpose, which is a generalization of the ε-contamination model [11] and has been shown to provide a good trade-off between flexibility and tractability [6], [7]. It is given by

$$\begin{aligned} \mathcal{F}_0 &= \{p_0 \mid p_0'(x) \le p_0(x) \le p_0''(x)\,\}, \\ \mathcal{F}_1 &= \{p_1 \mid p_1'(x) \le p_1(x) \le p_1''(x)\,\}, \end{aligned} \tag{5}$$

where p_k' and p_k'' denote lower and upper bounds on the true density, respectively. For the problem at hand, the bounds need to be non-negative functions satisfying $\int_0^1 p_k'(x)\, dx \le 1 \le \int_0^1 p_k''(x)\, dx$, $k = 0, 1$, but can otherwise be chosen freely by the test designer.

In principle, a minimax robust test is designed by finding a pair of densities $(g_0, g_1) \in \mathcal{F}_0 \times \mathcal{F}_1$ that is *least favorable* in the sense that it simultaneously maximizes both error probabilities among all feasible densities. If such a pair exists, the corresponding minimax optimal test can be shown to be a threshold test whose test statistic is the likelihood ratio of least favorable densities [7], [11]. In [7], it is shown that the least favorable densities (LFDs) for the band model can in general be written as

$$\begin{aligned} g_0(x) &= \min\left\{p_0''(x)\,,\, \max\left\{a_0\, g_1(x),\, p_0'(x)\right\}\right\}, \\ g_1(x) &= \min\left\{p_1''(x)\,,\, \max\left\{a_1\, g_0(x),\, p_1'(x)\right\}\right\}, \end{aligned} \tag{6}$$

where the two constants a_0 and a_1 have to be calculated such that the LFDs are valid densities, i.e., they integrate to one. Based on the procedure outlined in [7], an iterative algorithm to construct the LFDs is given in Algorithm 1. Starting with an initial guess for the LFDs $(g_0^0,\, g_1^0)$, the algorithm alternately updates g_0^i and g_1^i by finding a root of

$$f_k(a; g) = \int \min\{p_k''(x),\, \max\{a\, g(x),\, p_k'(x)\}\}\, dx - 1, \tag{7}$$

which, for a given density g, is a non-decreasing function of the scalar a. The iteration is terminated once both densities have converged within a tolerance δ.

Algorithm 1 Iterative procedure to calculate the least favorable densities

Input: p_0', p_0'', p_1', p_1'', g_0^0, g_1^0, δ

```
i ← 0
while true:
    a_0   ← root of f_0(a; g_1^i)
    g_0^{i+1} ← min{p_0'', max{a_0 g_1^i, p_0'}}
    a_1   ← root of f_1(a; g_0^{i+1})
    g_1^{i+1} ← min{p_1'', max{a_1 g_0^{i+1}, p_1'}}
    if ||g_0^i − g_0^{i+1}|| < δ and ||g_1^i − g_1^{i+1}|| < δ then
        break
    g_0^i ← g_0^{i+1},   g_1^i ← g_1^{i+1},   i ← i + 1
```

Output: g_0^i, g_1^i

Having calculated the LFDs, the robust LRT is then of the form (1), with the parametric densities (p_0, p_1) replaced by the LFDs (g_0, g_1).

IV. Numerical Results

In order to obtain the parameter estimates and density bands required to perform the two LRTs discussed in the the previous section, we use two training images named as A_1 and A_2

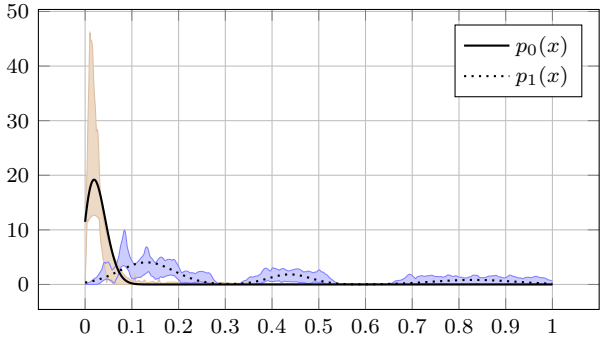

(a)

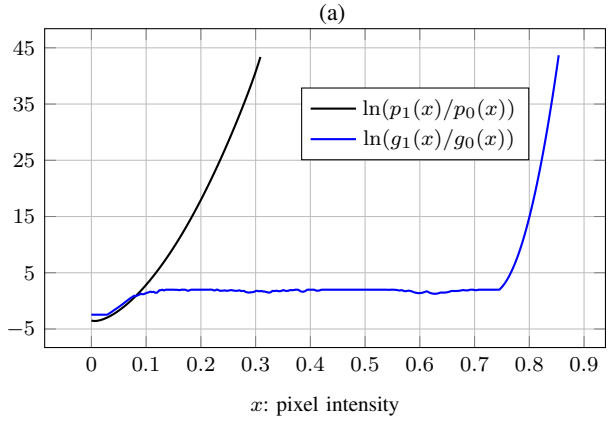

(b)

Fig. 4: (a) Parametric densities (p_0, p_1) and the constructed band model given in (9). (b) The likelihood ratio in logarithmic scale: parametric model (black), robust model (red).

generated by the NAFDTD software. The training image A_1 is a clutter-free tomographic image obtained from a nine-target scenario with flat ground surface. Given the center points of the nine target positions, we obtain a set of target pixels $\mathcal{X}_1$ by employing a region growing algorithm [12] to locate the target pixels in the training image A_1. From the training image A_2, which is a target-free tomographic image in the presence of rough ground surface, we obtain a set of clutter pixels $\mathcal{X}_0$. For the parametric LRT, the sets $\mathcal{X}_0$ and $\mathcal{X}_1$ are needed to obtain maximum likelihood estimates for the parameters of $p_0(x)$ and $p_1(x)$ in (3). The Rayleigh parameter is obtained as $\hat{\sigma_0} = 0.024$ and the 3-component Gaussian parameters are obtained as $\hat{\omega}_n = \{0.603, 0.210, 0.186\}$, $\hat{\mu}_n = \{0.118, 0.393, 0.808\}$, $\hat{\sigma}_n = \{0.051, 0.054, 0.105\}$. The resulting parametric density estimates are shown in Fig. 4a.

For the proposed robust detector, we construct the density bands via bootstrapping [13] and kernel density estimation. By bootstrapping the training data sets $\mathcal{X}_0$ and $\mathcal{X}_1$, we collect B new data sets $\{\tilde{\mathcal{X}}_{01}, \ldots, \tilde{\mathcal{X}}_{0B}\}$ and $\{\tilde{\mathcal{X}}_{11}, \ldots, \tilde{\mathcal{X}}_{1B}\}$. A kernel density estimator with a Gaussian basis function is then applied to each bootstrapped data set as follow

$$\hat{p}(\tilde{\mathcal{X}}_{kl}) = \frac{1}{Nh\sqrt{2\pi}} \sum_{n=1}^{N} \exp\left(-\left(\tfrac{x-y_n}{4h}\right)^2\right), \quad \forall y \in \tilde{\mathcal{X}}_{kl}, \quad (8)$$

where $k \in \{0, 1\}$, $l \in \{1, ..., B\}$, N is the number of elements in the data set $\tilde{\mathcal{X}}_{kl}$, and the smoothing parameter h needs to be chosen by the test designer. Here, we use the cross validation maximum likelihood method [14]. Subsequently, the lower and upper bounds in (5) are determined as the point wise minimum and maximum of all density estimates, i.e.,

$$\begin{aligned} \hat{p}'_k(x) &= \min\{\hat{p}(\tilde{\mathcal{X}}_{k1}), \hat{p}(\tilde{\mathcal{X}}_{k2}), ..., \hat{p}(\tilde{\mathcal{X}}_{kB})\}, \\ \hat{p}''_k(x) &= \max\{\hat{p}(\tilde{\mathcal{X}}_{k1}), \hat{p}(\tilde{\mathcal{X}}_{k2}), ..., \hat{p}(\tilde{\mathcal{X}}_{kB})\}. \end{aligned} \quad (9)$$

For our experiments, we calculate, under each hypothesis, $B = 500$ bootstrap estimates of the densities by randomly drawing (with replacement) $N = 400$ samples from the original data sets ($\mathcal{X}_0$, $\mathcal{X}_1$). This results in the density bands shown in Fig. 4a. As can be seen, almost all parts of the parametric densities lie inside the bands. We, hence, conjecture that under ideal conditions the pixel distribution indeed follows the parametric model; however, the actual measurements can contribute some random deviations of the distributions.

Given the density bands, the LFDs (g_0, g_1) are iteratively constructed using Algorithm 1. We set the initial densities (g_0^0, g_1^0) to 1.1 times their lower bounds ($\hat{p}'_0$, $\hat{p}'_1$), respectively. The iteration is terminated at the tolerance value $\delta = 0.001$. The log-likelihood ratio of the LFDs is shown in Fig. 4b. Compared with the case of no uncertainty (parametric model), the robust test statistic does not show a sharp increase for higher intensity values, but admits a large plateau of moderate significance values at approximately $0.124 \leq x \leq 0.745$. A high significance is only attributed to intensity values that exceed this range. This type of robust test has also been observed in [15] and [7], where it is shown that it corresponds to uncertainty sets that allow for smooth variations of the shapes of the distributions, but no gross outliers, which is the case for the given training data. In order to take outliers into account as well, we can let $p''_0, p''_1 \to \infty$, turning the band model into the ε-contamination model [7], [11]. Results for both the band model as well as the ε-contamination model are presented in the next section, where the robust detector is compared with the parametric detector.

Detection Results

The detection results are presented in a binary image whose pixels are given by

$$F(i,j) = \begin{cases} 1 & \text{when} \quad L(i,j) > \gamma \\ 0 & \text{when} \quad L(i,j) \leq \gamma, \end{cases} \quad (10)$$

where $1 \leq i \leq N_x$ and $1 \leq j \leq N_y$. For assessing the performance of the robust LRT, we compare its results to those from the parametric approach. The resulting binary image for a false alarm rate of $\alpha = 0.01$ is shown Fig. 5a, where correctly detected target regions are marked in red, false alarms are marked in black, and blue circles are used to

mark the miss detections. As seen, six targets are successfully detected, but three targets are missed. This result shows the disadvantage of trying to estimate a single distribution under each hypothesis which causes even small deviations in the distribution to degrade the detection performance.

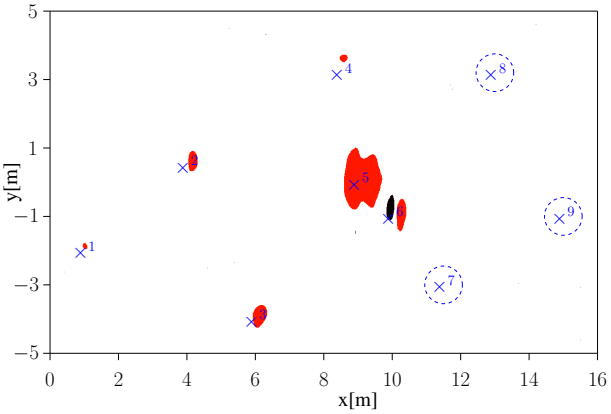

(a)

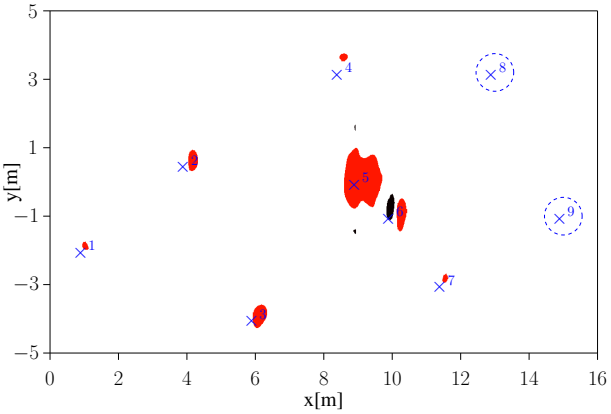

(b)

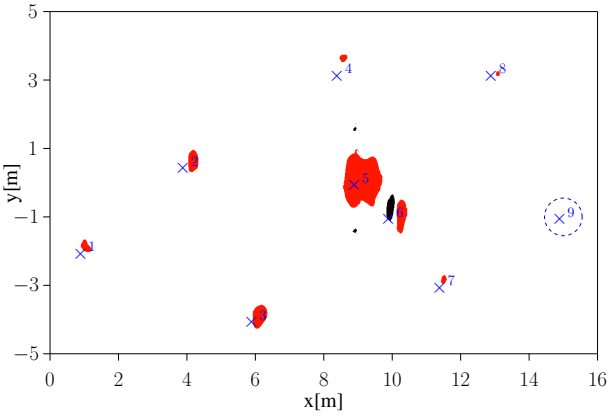

(c)

Fig. 5: Detection results for $\alpha = 0.01$. Color coding: detected targets (red), false alarm (black), miss detection (circle). (a) parametric test. (b) first robust test. (c) second robust test.

Fig. 5b shows the binary image of the robust detector using the log-likelihood depicted in Fig. 4b as a test statistic. In comparison to the parametric model, the robust LRT can detect one more target, namely the metallic $155\,\mathrm{mm}$ shell. Furthermore, using the ε-contamination model, which accommodates more uncertainty since $(p_0'', p_1'' \to \infty)$, only one target is missed, which is a buried plastic landmine located at the farthest downrange location as shown in Fig. 5c. We conjecture that these results can be further improvement by carefully choosing the density bands such that they better capture the type of uncertainties in the distributions. After all, the performance of a minimax optimal test critically depends on an adequate uncertainty model.

V. Conclusion

The problem of landmine detection with FL-GPR in a rough surface environment has been considered. We have presented a robust likelihood ratio test which is designed by first constructing a density band under each hypothesis using a kernel density estimator and then finding the corresponding least favorable densities. The performance of the robust detector has been evaluated using electromagnetic modeled data and has been compared with an alternative parametric approach. The robust detector was shown to reduce the influence of clutter and increase the detection accuracy.

References

[1] M. Ressler, L. Nguyen, F. Koenig, D. Wong, and G. Smith, "The army research laboratory (ARL) synchronous impulse reconstruction (SIRE) forward-looking radar," Proc. SPIE, vol. 656105, May 2007.

[2] T. Dogaru, "NAFDTD–A near-field finite difference time domain solver," U.S. Army Res. Lab., Adelphi, MD, USA, Tech. Rep. ARL-TR-6110, Sep. 2012, accessed on Feb. 14, 2017. [Online].

[3] D. Comite, F. Ahmad, D. Liao, T. Dogaru, and M.G.Amin, "Multi-view imaging for low-signature target detection in rough-surface clutter environment," IEEE Trans. Geosci. Remote Sens., vol. 55, no. 9, pp. 5220-5229, 2017.

[4] D. Comite, F. Ahmad, D. Liao, T. Dogaru, and M.G.Amin, "Adaptive detection of low-signature targets in forward-looking GPR Imagery," IEEE Trans. Geosci. Remote Sens. Lett., vol. 15, no. 10, pp. 1520-1524, October 2018.

[5] A. M. Zoubir, V. Koivunen, E. Ollila, and M. Muma, "Robust statistics for signal processing," Cambridge, United Kingdom: Cambridge University Press, 2018.

[6] S. A. Kassam, "Robust hypothesis testing for bounded classes of probability densities," IEEE Trans. Inform. Theory, vol.27, no. 2, pp. 242-247, 1981.

[7] M. Fauß and A. M. Zoubir, "Old bands, new tracks—revisiting the band model for robust hypothesis testing," IEEE Trans. Signal Processing, vol. 64, no. 22, pp. 5875-5884, 2016.

[8] A.D. Pambudi, M. Fauß and A. M. Zoubir, "Kernel-based cooperative robust sequential hypothesis testing," in Proc. IEEE ICSigSys, 2018, pp. 42-46.

[9] E. L. Lehmann and J. P. Romano, "Testing statistical hypotheses," 3rd ed. New York, NY, USA: Springer, 2005.

[10] C. H. Seng, A. Bouzerdoum, M. G. Amin, and F. Ahmad, "A Gaussian-Rayleigh mixture modeling approach for through-the-wall radar image segmentation," in Proc. IEEE Int. Conf. Acoust., Speech Signal Process., Kyoto, Japan, Mar. 2012, pp. 877-880.

[11] P. J. Huber, "A robust version of the probability ratio test," Ann. Math. Stat., vol. 36, no. 6, pp. 1753-1758, 1965.

[12] R. Adams and L. Bischof, "Seeded region growing," IEEE Trans. Pattern Anal. Mach. Intell., vol. 16, no. 6, pp. 641-647, Jun. 1994.

[13] A. M. Zoubir and D. R. Iskander, "Bootstrap techniques for signal processing," Cambridge, United Kingdom: Cambridge University Press, 2007.

[14] Q. Li and J. S. Racine, "Nonparametric econometrics: theory and practice," Princeton University Press, 2007.

[15] G. Gül, A. M. Zoubir, "Minimax robust hypothesis testing," IEEE Trans. Information Theory., vol. 63, no. 9, pp. 5572-5587, April 2017.